IOPscience iopscience.iop.org

Home Search Collections Journals About Contact us My IOPscience

Application of coupled nanoscale resonators for spectral sensing

This article has been downloaded from IOPscience. Please scroll down to see the full text article.

2009 J. Phys.: Condens. Matter 21 144213

(http://iopscience.iop.org/0953-8984/21/14/144213)

View the table of contents for this issue, or go to the journal homepage for more

Download details:
IP Address: 129.252.86.83
The article was downloaded on 29/05/2010 at 18:56

Please note that terms and conditions apply.

J. Phys.: Condens. Matter **21** (2009) 144213 (10pp) doi:10.1088/0953-8984/21/14/144213

Application of coupled nanoscale resonators for spectral sensing

N Nefedov

Nokia Research Center, Hardturmstrasse 253, CH-8005 Zurich, Switzerland
and
Swiss Federal Institute of Technology Zurich (ETHZ), ISI Laboratory, Sternwartstrasse 7, CH-8092 Zürich, Switzerland

E-mail: nikolai.nefedov@nokia.com

Received 12 July 2008, in final form 18 November 2008
Published 18 March 2009
Online at stacks.iop.org/JPhysCM/21/144213

Abstract
In this paper we propose a method to perform tunable spectral sensing using globally inhibitory coupled oscillators. The suggested system may operate in the analog radio frequency (RF) domain without high speed ADC and heavy digital signal processing. Oscillator arrays may be made of imprecise elements such as nanoresonators. Provided there is a proper coupling, the system dynamics can be made stable despite the imprecision of the components. Global coupling could be implemented using a common load and controlled by digital means to tune the bandwidth. This method may be used for spectral sensing in cognitive radio terminals.

(Some figures in this article are in colour only in the electronic version)

1. Introduction

Development of high data rate communication systems requires implementation of complicated algorithms operating at high speed with low power consumption. Despite the progress in digital CMOS technology, high data rate digital processing poses a number of problems both for signal digitizing and its processing. These problems motivate a search for new architectures capable of combining advances in scaling, new materials and information processing at the nanoscale. Currently there is growing interest in development of signal processing systems using nanoscale devices such as molecular electronics, nanowires, nanomechanical systems, etc [1–10]. For example, scaling MEMS to the nanoscale gave rise to low power nano-electromechanical systems (NEMS) with operational frequencies above the GHz (frequency range typical for modern communication systems) [6, 7].

Recent advances in nanotechnology and scaling allow us to build systems with a large number of nanoresonators (such as CNT-based NEMS [9]) integrated within a CMOS chip. On the other hand, scaling poses a problem to maintain the accuracy of the elements.

A practical way to cope with inaccuracy may be seen in building hybrid systems combining low precision analog/nano-components with digital calibration/control. Besides, in network structures one may use a proper coupling such that the system dynamics may be made stable despite the imprecision of components [11]. In particular, collective behavior of coupled NEMS networks with the assistance of coupling and calibration provided by digital CMOS may allow us to implement low power information processing algorithms in the analog domain with digital calibration/control. For example, it makes feasible spectral processing in the RF domain which is of special importance for high data rate wireless communications systems. The suggested method may be used for spectral sensing in cognitive radio terminals [12, 13], where wide radio spectrum bands are to be repeatedly scanned in real-time with low power consumption.

This paper is organized as follows. Section 2 provides a background on coupled oscillators. The proposed method of spectral sensing based on inhibitory globally coupled arrays and its possible NEMS implementation are outlined in section 3 and section 4, respectively; conclusions follow in section 5.

2. Coupled oscillators

2.1. Background

Coupled oscillators have been under intensive studies in different fields of science for decades (e.g. see [11, 14–16]). In this section we introduce a notation and outline the basic

 © 2009 IOP Publishing Ltd Printed in the UK

concepts used in the following. We consider weak coupling among oscillators (active rotators) such that they maintain their limit-cycle trajectories perturbed by coupling. It allows us to ignore the coupling effect on an oscillator's amplitude and describe the system only with phase relationships such as

$$\frac{\mathrm{d}\theta_n}{\mathrm{d}t} = \omega_n + Q_n(\theta_1, \theta_2, \ldots, \theta_N); \qquad n = 1, \ldots, N \quad (1)$$

where ω_n is the partial (uncoupled) frequency of the nth oscillator and Q_n presents a coupling effect on phase θ_n from all other oscillators and is described as 2π-periodic in each of its arguments. We present coupling as an interaction among all pairs of oscillators, $Q_n(\theta_1, \theta_2, \ldots, \theta_N) = \sum_{m=1}^{N} q_{nm}(\theta_m, \theta_n)$. In the case of weak coupling $q_{nm}(\theta_m, \theta_n) = q_{nm}(\theta_m - \theta_n)$ and $q_{nm}(0) = 0$, i.e. there are no interactions if identical oscillators are in phase. Such coupling is known as diffusive coupling and is described as

$$\frac{\mathrm{d}\theta_n}{\mathrm{d}t} = \omega_n + \sum_{m=1}^{N} q_{nm}(\theta_m - \theta_n). \quad (2)$$

A special case of (2), $q_{nm}(\theta) = (k/N)\sin(\theta)$, corresponds to uniform all-to-all coupling with strength k among N oscillators and is known as the global phase-coupled Kuramoto model [14] [15]:

$$\frac{\mathrm{d}\theta_n}{\mathrm{d}t} = \omega_n + \frac{k}{N}\sum_{m=1}^{N} \sin(\theta_m - \theta_n); \qquad n = 1, \ldots, N. \quad (3)$$

Global coupling may be seen as the complex mean field $R(t)$ acting on a selected oscillator. Then (3) may be rewritten as

$$\frac{\mathrm{d}\theta_n}{\mathrm{d}t} = \omega_n + kr\sin(\psi - \theta_n) \quad (4)$$

where the mean field is defined by

$$R(t) = r(t)\mathrm{e}^{\mathrm{i}\psi(t)} = \frac{1}{N}\sum_{n=1}^{N} \mathrm{e}^{\mathrm{i}\theta_n(t)}; \quad (5)$$

where r and ψ are the mean-field amplitude and phase, respectively. Depending on k, coupling may be attractive ($k > 0$) or repulsive ($k < 0$).

2.2. Oscillators with attractive global coupling

Attractive coupling is observed in many natural phenomena and is the topic for extensive studies. For example, it is shown that oscillator arrays with different partial frequencies may be driven into a collective behavior without external force provided that positive coupling strength k is large enough compared to frequency variations σ_ω [14, 15]. Then the system evolves from quasi-chaotic to partial synchronization, where oscillators with close frequencies are frequency-locked, resulting in a growing mean field which in turn attracts further staying apart (in frequency) oscillators into the frequency lock. If identical oscillators are all in phase-sync, it results in maximum mean-field amplitude ($r = 1$), while the mean field formed by oscillators with random phases approaches zero ($r \to 0$). For this reason the mean-field amplitude r is also referred to as the order factor.

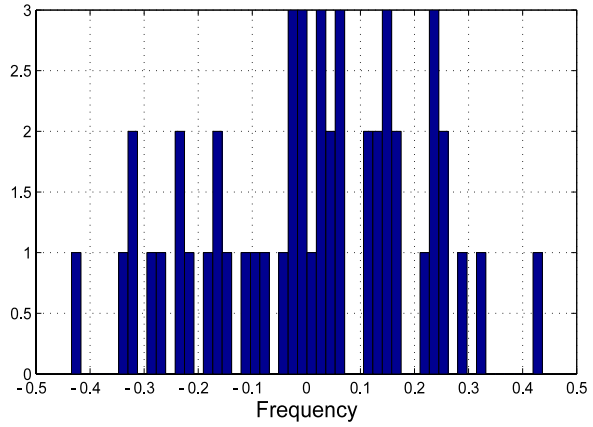

Figure 1. Distribution of frequencies in oscillator array, variance $\sigma_\omega^2 = 0.02$, $N = 50$.

In practice the oscillators' frequencies are not identical, resulting in complicated dynamics. In the following we consider Gaussian frequency distribution $g(\omega)$ with zero mean and variance σ_ω^2; an example of the frequency distribution for $N = 50$ and $\sigma_\omega^2 = 0.02$ used in simulations below is shown in figure 1. Note that oscillators with partial frequencies $|\omega_n - \omega_0| > kr$ cannot be attracted to the frequency lock; it results in partial frequency synchronization and the lower steady state order factor $r < 1$. Furthermore, even if all oscillators with different frequencies are synchronized, it results at best in phase-mode locking (constant phase difference), but not in phase synchronization (where the phase difference is zero). Phase-mode locking among oscillators results in a fluctuating order factor with variance proportional to N^{-1}.

The effect of frequency synchronization in a globally attractively coupled system allows us to built fixed-frequency oscillators from NEMS resonators with randomly spread frequencies.

3. Spectral sensing with coupled oscillator arrays

3.1. Inhibitory coupled oscillators

Convergence to the frequency sync (measured by the order factor) in oscillator arrays with attractive coupling depends mainly on the coupling strength. This phenomenon masks external excitations and limits signal processing possibilities. To make coupled oscillators to be more sensitive for external excitations we suggest translating external signals into coupling strength. However, before this mapping we need to keep the system out of sync when no external signal is present. It can be done by utilizing *inhibitory* (or repulsive) coupling, preventing the system falling into a collective behavior. Then, once the external excitation is above the inhibitory coupling, it forces the system, proportional to the strength of the external excitation, to move into more ordered behavior.

To analyze the mean-field behavior phase equations (4) may be transformed into mean-field equations by multiplying (3) by $\mathrm{e}^{\mathrm{i}\theta_m}$ and summing over m, which for non-identical

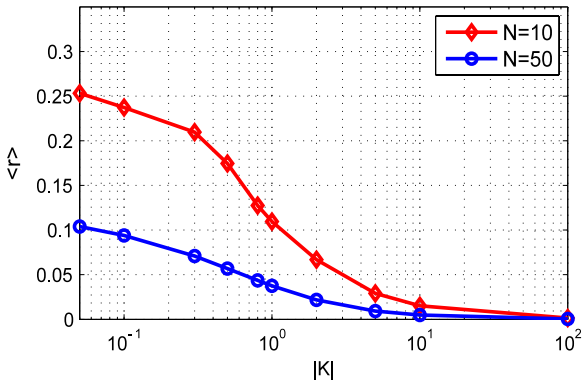

Figure 2. Dependence of averaged mean field $\langle r(t)\rangle$ from repulsive coupling strength, $k < 0$.

frequencies finally gives [17]

$$\dot{R} = \frac{1}{N}\sum_n \omega_n e^{i\theta_n} + \frac{k}{2}\left[R - R^*\frac{1}{N}\sum_n e^{i2\theta_n}\right]. \qquad (6)$$

For large N (in simulations for $N > 4$), the eigenvalues of the synchronized solution are positive, hence the synchronized solution is unstable.

In the case of identical oscillators ($\omega_n = \omega_0$) with inhibitory global coupling the mean field approaches zero from any initial condition at negative coupling strength $k < 0$. The resulting phase distribution is not unique: there may be multiple phase distributions among individual oscillators subject to the constraint $\sum_n e^{i\theta_n} = 0$. It may be shown that all these solutions are neutrally stable.

For oscillators with non-identical frequencies there are multiple solutions for (6) and the mean field oscillates at small values of inhibitory coupling: partial frequencies of oscillators are preserved on average, while inhibitory coupling adjusts its phases to minimize the mean field. In the limit $N \to \infty$ it is shown that standard deviation of mean-field fluctuations is proportional to $N^{-1/2}$ [17]. As an example, figure 2 presents the averaged mean field as a function of repulsive coupling strength. These curves are obtained by numerical solution of (4) with frequency distribution $g(\omega)$ shown in figure 1. Time evolution of randomly initialized frequencies for globally repulsively coupled ($k = -0.5$) oscillators is shown in figure 3(a). Note that the oscillators' frequencies on average are kept unchanged, but the increased repulsive coupling is smoothing the discrete spectrum by affecting the oscillators' phases and resulting in quasi-chaotic behavior.

3.2. Forced oscillations

Models for phase-coupled oscillators (1) may be extended to include external field Q_F:

$$\frac{d\theta_n}{dt} = \omega_n + Q_n(\theta_1, \theta_2, \ldots, \theta_N) + Q_F(\theta_1^{ext}, \theta_2^{ext}, \ldots, \theta_M^{ext});$$
$$n = 1, \ldots, N; \quad M \leqslant N, \qquad (7)$$

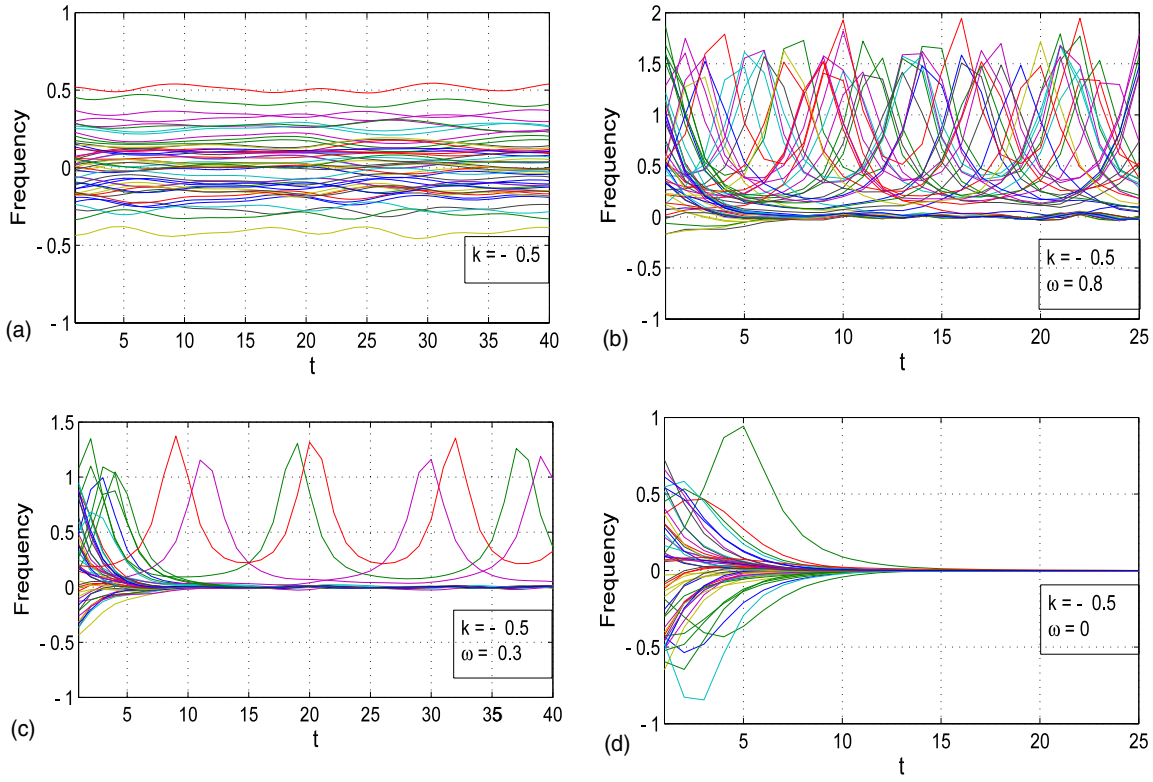

Figure 3. Time evolution of randomly initialized frequencies ($\sum_{n=1}^{N} \omega_n = \omega_0 = 0$) for globally repulsively coupled ($k = -0.5$) oscillators without and with external periodic forcing $A_{ext}\sin(\omega_{ext}t)$, $\delta\omega = \omega_{ext} - \omega_0$: (a) no forcing $A_{ext} = 0$; (b) $\delta\omega = 0.8$, $A_{ext} = 1$, quasi-chaotic behavior; (c) $\delta\omega = 0.3$, partial sync; (d) $\delta\omega = 0$, frequency sync.

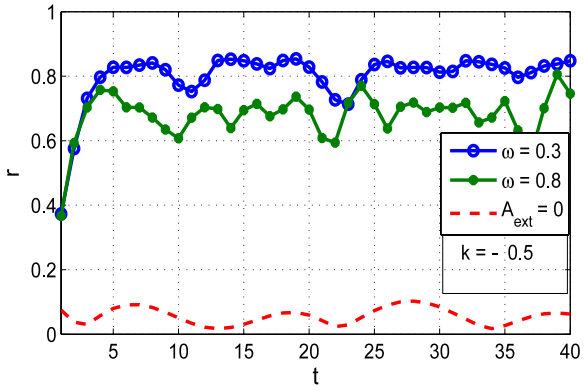

Figure 4. Evolution of mean-field amplitude $r(t)$ in time under different time-periodic forcing $A_{\rm ext}\sin(\omega_{\rm ext}t)$, $\delta\omega = \omega_{\rm ext} - \omega_0 : A_{\rm ext} = 1$, $\delta\omega = 0.3, 0.8$; $N = 50$.

where Q_F is a 2π-periodic function in all of its arguments. Based on (3) we may write for time-periodic external forcing

$$\frac{{\rm d}\theta_n}{{\rm d}t} = \omega_n + kr\sin(\psi - \theta_n) + q_n^{\rm ext}\sin(\theta_n^{\rm ext}) \quad n = 1, \ldots, N. \tag{8}$$

The last term in (8) may be presented as $A_n\sin(\theta_n - \omega_{\rm ext}t)$, where A_n and $\omega_{\rm ext}$ are the amplitude and frequency of the external force. Introducing a new variable $\varphi_n = \theta_n - \omega_{\rm ext}t$ we obtain again equation (8) for φ_n, but with other frequencies $\tilde{\omega}_n = \omega_n - \omega_{\rm ext}$:

$$\frac{{\rm d}\varphi_n}{{\rm d}t} = \tilde{\omega}_n + kr\sin(\psi - \varphi_n) + A_n\sin(\phi_n - \varphi_n) \quad n = 1, \ldots, N. \tag{9}$$

In other words, time-periodic external forcing may be presented as a modification of the distribution $g(\omega)$ of partial frequencies in the oscillator array.

As an illustration, time evolution of frequencies of inhibitory coupled oscillators under different periodic forcing are depicted in figures 3(b)–(d). When the forcing frequency $\omega_{\rm ext}$ is approaching the average frequency of the oscillator array, $\omega_0 = \sum_{n=1}^{N}\omega_n = 0$, the excitation strength $A_n = A_{\rm ext}$ overcomes the repulsive coupling k and the system evolves from quasi-chaotic (figure 3(b)) to partial synchronization (figure 3(c)), where oscillators with frequencies close to $\omega_{\rm ext}$ are attracted to the frequency lock, resulting in a growing order factor $\langle r(t)\rangle$. Recall that for non-identical oscillators the mean field is not constant. Evolution of mean-field amplitude $r(t)$ in time at different frequencies of periodic forcing $\omega_{\rm ext}$ is depicted in figure 4. As one may see the order factor $\langle r(t)\rangle$ depends on the frequency of external forcing, we use this property in the following for spectrum sensing.

In the general case the external field is described by a probability density $f(A_n, \phi_n)$ and includes a white-noise forcing term ξ_n. Then the resulting stochastic equations are

$$\frac{{\rm d}\varphi_n}{{\rm d}t} = \tilde{\omega}_n + kr\sin(\psi - \varphi_n) + A_n\sin(\phi_n - \varphi_n) + \xi_n \quad n = 1, \ldots, N \tag{10}$$

where ξ_n is an independent stochastic process with expected values $\langle\xi_n(t)\rangle = 0$ and $\langle\xi_n(s)\xi_m(t)\rangle = 2D\delta_{nm}\delta(s-t)$.

Besides external fields, time delays in interactions, e.g. due to signal propagation through band-limited circuits, may significantly change the system dynamics. To make the model more realistic we also include time delays in coupling among oscillators, τ_{nm}, into the resulting Langevin equations:

$$\frac{{\rm d}\varphi_n}{{\rm d}t} = \tilde{\omega}_n + \frac{k}{N}\sum_{m=1}^{N}\sin(\varphi_m(t-\tau_{nm}) - \varphi_n(t)) + A_n\sin(\phi_n - \varphi_n) + \xi_n. \tag{11}$$

The attractive coupling attempts to force in phase all oscillators whereas the frequency dispersion and the noise tend to destroy coherence. For negatively coupled oscillators with non-equal frequencies and external periodic forcing $\omega_{\rm ext} = \omega_0$, there will be fluctuations of mean field at any value of coupling. Oscillator phases and frequencies evolve from chaotic to partially sync as the amplitude of external force is increasing. Finally, a collective behavior may appear as a result of competition between external forcing and desynchronizing effects from inhibitory coupling, noise and partial frequencies dispersion.

Instead of tracking phases of individual oscillators in stochastic differential equations (11), it is convenient to describe the system in terms of a density function $\rho(\varphi, t)$ in the limit of infinite number of oscillators N and consider associated Fokker–Planck equations (FPE) (see appendix A).

Analyzing density functions we can observe that increasing positive coupling above a critical coupling $k_{\rm c}$ makes the density function more picky, creating frequency synchronization among non-identical oscillators and increasing mean field; in the case of identical oscillators ρ approaches the delta function (phase synchronization). On the other hand, the repulsive coupling tends to a flat density function and reinforces incoherence even in the case of oscillators with identical frequencies. It may be shown that the incoherence remains linearly stable as long as $k < k_{\rm c}$. Structured external field then imposes a regular behavior, reshapes the flat distribution and changes the mean field according to applied forcing frequency and amplitude. The presence of noise reduces the order parameter.

The FPE allows us to consider arbitrary external fields in the limit $N \to \infty$ (see appendix A). To evaluate finite-N dynamics, we calculated solutions for inhibitory coupled oscillators using FPE (A.7) and using (9)–(11) for cases with periodic forcing. We found a good correspondence between averaged mean fields in both cases. It allowed us to use FPE to calculate order factors for finite numbers of oscillators in the following.

Dependence of order factor from amplitude $A_{\rm ext}$ of external periodic forcing $\omega_{\rm ext} = \omega_0$ at different coupling strength is shown in figure 5. As one can see, the order factor $\langle r\rangle$ depends monotonically from the amplitude of the external force at fixed coupling. This property may be used for energy sensing of external signals addressed below. Figure 6 shows the order factor for global inhibitory coupled oscillators ($k = -1$) with different amplitude–frequency characteristics of forcing. Similar results are reported in [18].

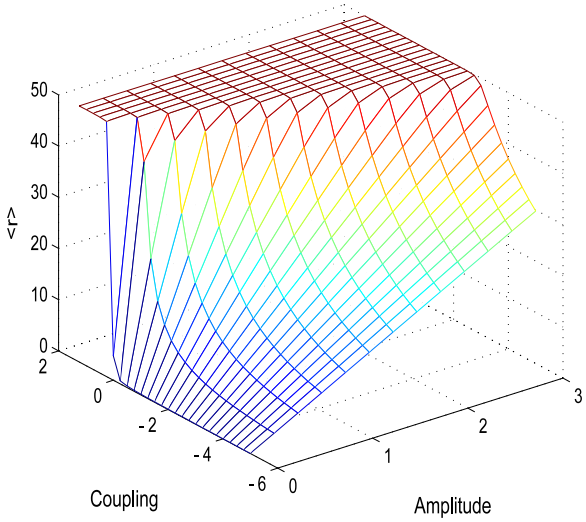

Figure 5. Order factor of coupled oscillators as a function of coupling and the amplitude of forcing signal $\omega_{\text{ext}} = \omega_0$.

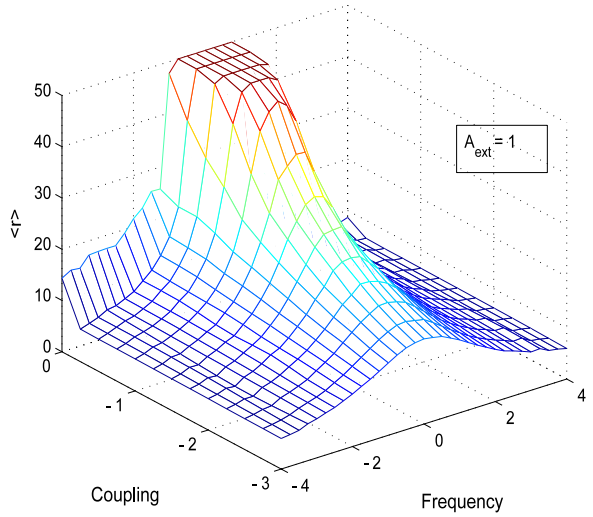

Figure 7. Order factor of coupled oscillators as a function of coupling and frequency of forcing signal, $A_{\text{ext}} = 1$.

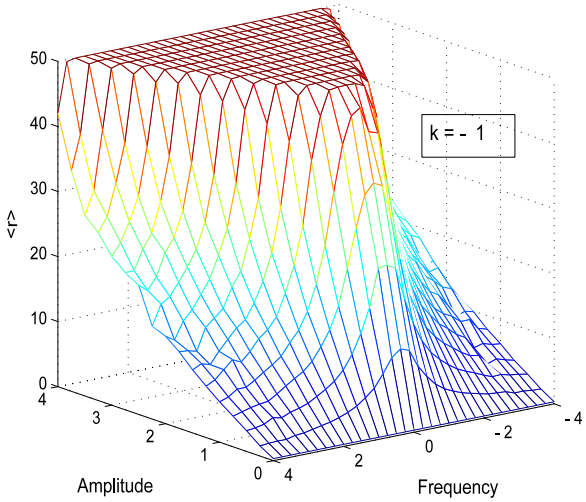

Figure 6. Order factor of coupled oscillators ($k = -1$) as a function of amplitude and frequency of forcing signal.

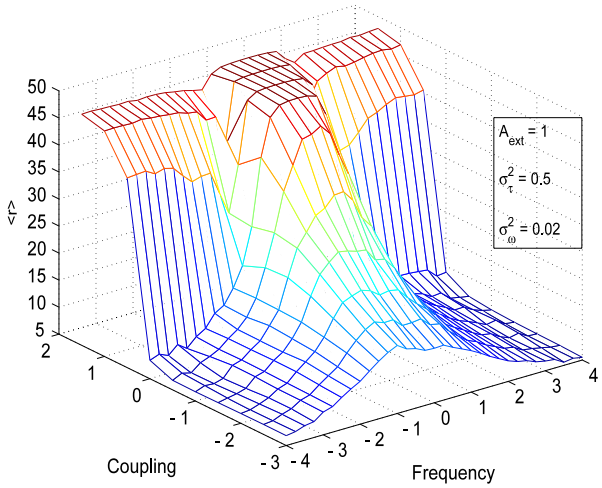

Figure 8. Order factor of coupled oscillators in presence of delays as function of coupling and frequency of forcing signal, $A_{\text{ext}} = 1$.

The order factor of coupled oscillators as a function of frequency of the forcing signal with fixed amplitude $A_{\text{ext}} = 1$ at different coupling levels is depicted in figure 7. As one may see, by adjusting coupling strength it is possible to tune the frequency bandwidth. It allows us to utilize amplitude–frequency selectivity and its dependence on tuning and the amplitude of external excitation for spectral sensing in radio systems (e.g. cognitive radio). Figure 8 presents simulations similar to figure 7, but with exponentially distributed random delays ($\sigma_\tau^2 = 0.5$) in coupling. This figure shows that the system is robust to time delays of the order ω_0^{-1} in coupling and preserves filtering properties (cf figure 7), provided that coupling remains repulsive. Note that $\omega_0 = 0$ in the figures above is a free parameter; another value of ω_0 results in the corresponding shift along the frequency axis. Below we outline a possible implementation of this kind of sensing with nanoscale resonators.

4. Nanoscale resonators for spectral sensing

4.1. General parameters of oscillator array

To implement the proposed scheme we need to map it onto physical devices (e.g. NEMS arrays). From figure 7 one may see that the best frequency selectivity is achieved when repulsive coupling ($k \simeq -0.3, \ldots, -1$) matches the amplitude of external excitation ($A_{\text{ext}} = 1$). This relation will be used in the following. The number of oscillators N is the design parameter and may be selected based on required accuracy and sensitivity. For example, in the absence of external signals for $N = 50$ oscillators with coupling $k \in [-0.3, -1]$, mean-field fluctuations are about 5% of the full scale (figure 2). One may obtain the same dynamical range, 5%, with $N = 10$ at $k = -2$ for a cost of lower frequency selectivity (cf figure 7); functionality of the array degrades significantly for $N < 10$.

The next step is to outline general parameters of oscillators. We model the oscillator as an active device with

a negative resistor R_a embedded into the serial resonant circuit with inductance L, resistor R_L and capacitor C. The negative resistance depends nonlinearly on the amplitude of oscillations $R_a = R_a(|V|)$. Under external forcing V_{ext} the oscillator dynamics is described by

$$\frac{dV}{dt} + \omega_0^2 \int V\,dt + \frac{\omega_0}{Q}\left(1 - \frac{R_a}{R_L}\right)V = \frac{\omega_0}{2Q}V_{ext} \tag{12}$$

$$V_{ext} = A_{ext}(t)e^{i(\omega_{ext}t+\phi(t))} = A_{ext}(t)e^{i\theta_{ext}(t)} \tag{13}$$

where V is complex (phasor) voltage and the embedded passive network is characterized by a Q factor. At a sufficiently high $Q > 10$, the output voltage is presented as $V = A(t)e^{i(\omega_0 t+\phi(t))} = A(t)e^{i\theta(t)}$. The saturation may be modeled as $1 - R_a/R_L \simeq \mu(A_0 - |V|^2)$, where μ describes nonlinearity and $A_0 = 1$ is the amplitude of free-running oscillations with frequency ω_0. It allows us to present (12) as a complex form of the forced Van der Pol oscillator (cf appendix B):

$$\frac{dV}{dt} + \frac{\mu\omega_0}{2Q}[(1 - |V|^2) + i\omega_0] = \frac{\omega_0}{2Q}V_{ext}. \tag{14}$$

Assuming a weak perturbation $|V_{ext}| \ll |V|$, the oscillator amplitude remains close to its limit cycle and the phase dynamics is described by

$$\begin{aligned}\frac{d\theta}{dt} &= \omega_0 + \frac{\omega_0}{2Q}\mathrm{Im}\left(\frac{V_{ext}}{V}\right)\\ &= \omega_0 + \frac{\omega_0}{2Q}\frac{A_{ext}}{A}\sin(\theta_{ext} - \theta).\end{aligned} \tag{15}$$

In a steady state the oscillator locks to the external excitation, $d\theta/dt = \omega_{ext}$, and (15) takes the form $\omega_{ext} - \omega_0 = \Delta\omega_{lock}\sin(\Delta\theta)$, where $\Delta\omega_{lock} = \frac{\omega_0}{2Q}\frac{A_{ext}}{A}$ is the oscillator locking bandwidth. Similarly, dynamics of N oscillators with global coupling strength $\tilde{k}$ is presented by

$$\frac{d\theta_n}{dt} = \omega_n + \tilde{k}\frac{\omega_0}{2Q}\sum_{m=1}^{N}\frac{\tilde{A}_m}{\tilde{A}_n}\sin(\theta_m - \theta_n). \tag{16}$$

In the case of identical amplitudes, $\tilde{A}_n = A_0$, the frequency synchronization of all oscillators, $d\theta_n/dt = \omega_0$, takes place provided attractive coupling $\tilde{k} > (Q/N)(\Delta\omega/\omega_0)$, where $\Delta\omega = \omega_{max} - \omega_{min}$. In other words, in the locking bandwidth (and hence the critical coupling strength) depends on the resonator quality, oscillators' amplitudes and applied excitations. Now we can map abstract values of coupling k used in the previous sections to physical parameters. As an example, let's consider $N = 100$ nanoresonators with $Q \approx 20$ (as reported for CNT at room temperature) in the frequency range $\Delta\omega = (1.1 - 0.9)$ GHz with average frequency $\omega_0 = \sum_{n=1}^{N}\omega_n/N = 1$ GHz. The coupled array will be forced by mutual entrainment to the average frequency ω_0 provided that more than 4% ($\tilde{k} > 0.04$) of each oscillator energy is allocated to the global coupling bath; it allows us to define parameters of the coupling network.

In a similar way we may map values of repulsive coupling shown in figures 5–8 into physical parameters. Recall that the purpose of repulsive coupling is to prevent falling into frequency synchronization in the absence of external signals, i.e. A_{ext}/A_0 and k are scaled to the same factor. For example, $k = -1$ was taken to prevent synchronization of all oscillators under external forcing $A_{ext}/A_0 < 1$. In practice $A_{ext} \ll A_0$ and coupling strength is scaled down accordingly (which is also required for weak phase coupling assumption in (15)).

Global coupling may be implemented as a common load similar to global coupling in Josephson junctions [19, 20]. In particular, we can obtain the mean field $R(t)$ by adding output currents and then reading off the feedback signal from a resistor divider (or using a gain-controlled operational amplifier, AO). Repulsive coupling may be implemented by placing an AO invertor into the feedback loop.

4.2. Possible implementation

Resonant nanostructures have been addressed in a number of papers. For example, parametric resonance in an electrostatically driven nanowire is studied in [4], laser-driven limit-cycle oscillators in NEMS resonators in different disc shapes and wires are reported in [8], mechanically coupled NEMS with resonant frequencies up to 18 MHz are presented in [21]. Besides silicon-based NEMS, carbon nanotubes (CNT) are currently under intensive studies because of their superior mechanical properties, small cross sections and possibility for defect-free self-assembling [3]. Additionally, the CNT can act as a transistor, may be able to sense its own motion and can be made CMOS compatible. Recently it is shown that CNTs can be used as nanoswitches [5] and as GHz oscillators [6, 7].

The proposed scheme is based on collective behavior of coupled low-accuracy oscillators and may be implemented with different technologies. Top-down fabricated beams [2] may be used to build oscillator arrays operating at the MHz range. Devices operating at higher frequencies (above 2 GHz) may be implemented using self-assembling technologies [22]. As a not-limiting example, in the context of modern communication systems at GHz range, we briefly outline a possible implementation using low-accuracy CNT resonators and preliminary estimate design parameters. More details on this ongoing project will be reported elsewhere.

Let us consider a suspended CNT clamped on both sides to metal pads (source and drain) and capacitively coupled to a gate as reported in [9]: tunable CNT-based NEMS is depicted at figure 9. Similar to MEMS, we may add a positive feedback loop that converts drain output current into voltage (I/V block at figure 9) which then is fed back to the gate to excite CNT resonance modes. Provided a proper positive feedback this structure may be used as a limit-cycle oscillator or rotator (shown in the upper-right corner at figure 9). Another, probably more appropriate, method to maintain GHz oscillations in CNT-based NEMS is to use ac voltage V_g^{ac} ($\omega_{par} \approx$ 200–300 MHz, $A_g^{ac} \approx 100$ mV) applied to the gate for parametric excitation of CNT eigenmodes at GHz range. This method could allow us to excite and maintain oscillations in the whole array of resonators. Additionally, dc voltage $V_g \approx 2$ V applied to the gate would allow to change CNT strain and hence to control the eigenmodes which may be excited by external ac source $V(\omega_{ext})$ [9]. The suspended nanotube

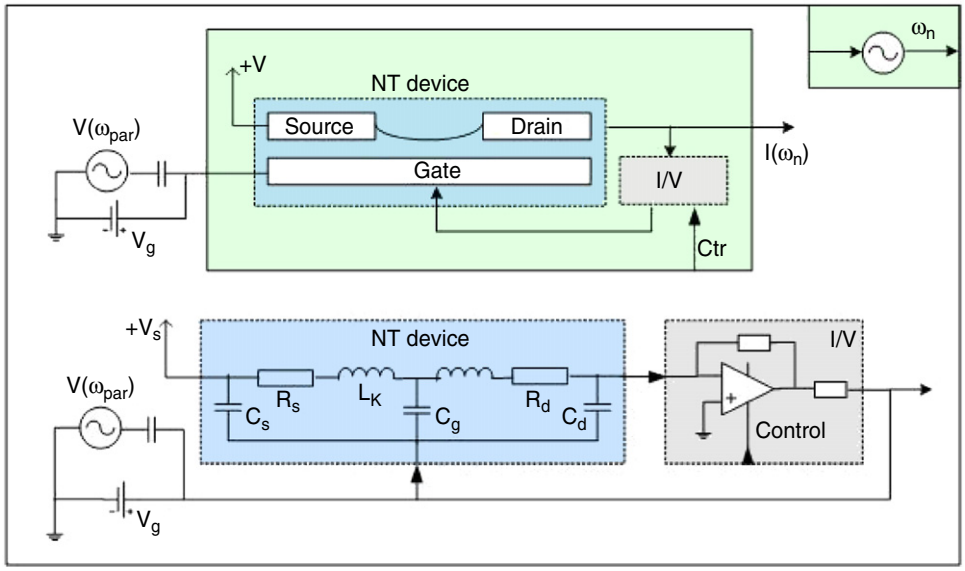

Figure 9. Tunable CNT-based NEMS oscillator (cf [9]): (top) block diagram; (bottom) the equivalent circuit schematic: preliminary estimates $R_s = R_d \approx 30$ kΩ, $C_g \approx 10$ aF, $L_K \sim$ nH μm^{-1}.

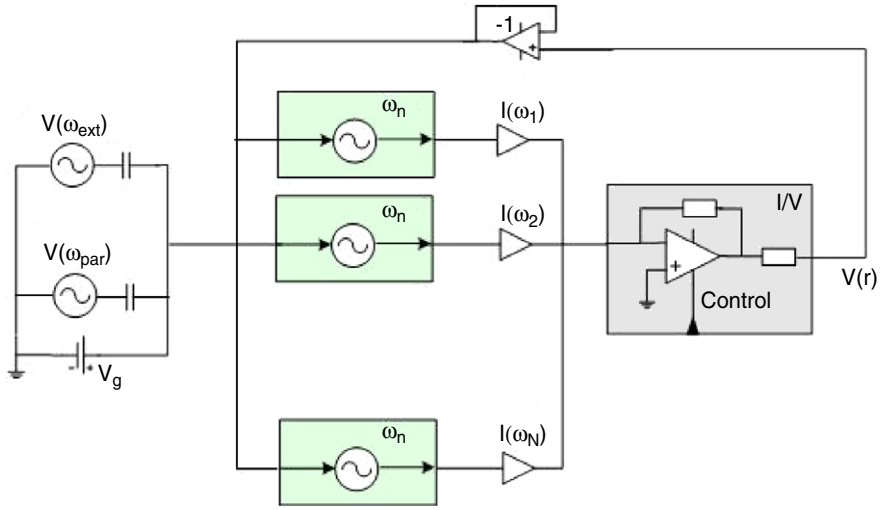

Figure 10. Array of oscillators with global coupling.

starts to oscillate when the driving frequency approaches CNT mechanical eigenmodes.

One-dimensional motion of a nanotube can be described by the Duffing equation [3]. It may be shown that, for small displacements and weak interactions, globally coupled Duffing oscillators may be described by (3) (see appendix B). Under these assumptions we may consider a system of *inhibitory* globally coupled oscillators shown in figure 10. Here current outputs from oscillators $I(\omega_n)$ are combined at a common load followed by the feedback via current/voltage conversion (I/V block at figure 10) creating global coupling. The amount and sign of the feedback may be controlled by operational amplifiers (OA) with tunable amplification, the estimated feedback voltage $V_{\rm fb} \approx 10$ mV. The same OA is used to block external signal leakage into the common load. In the absence of external signals the global negative feedback is to be (digitally) calibrated to prevent system convergence into frequency lock and keep the order parameter close to zero. Another possible way to implement feedback is to combine output voltage $V(r)$ after the I/V block with V_g which would allow us to modify (according to the feedback) mechanical eigenfrequencies for the whole bunch of nanotubes. Global coupling strength k may be digitally controlled to tune the bandwidth of spectral sensing (cf figure 7). CNT strain and its eigenmodes may be tuned by changing dc voltage V_g (figure 9). Tuning voltage gate V_g may be used to adjust the whole set of frequencies $\Omega = \{\omega_1, \ldots, \omega_N\}$ in a given oscillator array (figure 10).

Several oscillator arrays with different frequency sets Ω_n tuned by dc gate voltage V_g (to adjust frequency) and coupling k (to adjust bandwidth) may be used to make coarse spectral sensing as shown at figure 11. In particular, when voltage $V(r_{\Delta\Omega_n})$ corresponding to order factor(s) $r_{\Delta\Omega_n}$ of

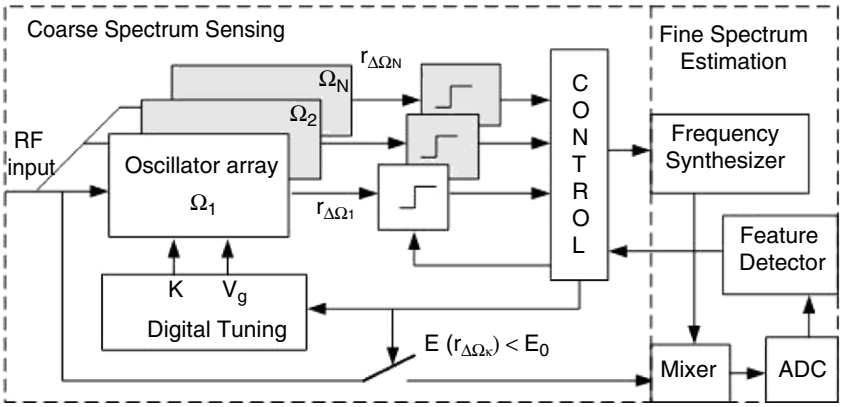

Figure 11. Tunable coupled oscillator arrays for spectral sensing.

some frequency band(s) is below a threshold E_0 (set by the control block), it indicates potential spectrum holes. Then control block sends information on a relevant frequency(s) band $\Delta\Omega_n$ to the frequency synthesizer which sets the relevant local frequency for the mixer; at the same time the input RF signal is connected to the mixer. After downconverting the baseband signal in a selected (relatively narrow) frequency band is digitized by ADC and then analyzed in the feature detector. If needed the feature detector may refine frequency and bandwidth of the oscillator array via feedback control.

5. Conclusions

In this paper we present the method of coarse spectral sensing in analog domain using globally coupled limit-cycle oscillators which may be made of imprecise nanoscale components such as CNT-based NEMS or top-down fabricated beams. Provided there is proper inhibitory coupling, the system's collective behavior (measured by order factor) becomes sensitive to amplitude and frequency content of excitation and digital control of coupling allows us to tune the spectral sensing position and bandwidth. This method may be used in cognitive radio terminals.

Appendix A

A convenient way to deal with a set of Langevin equations (10) and (11) is to introduce a one-oscillator probability density $\rho_n(\varphi, t) \triangleq \rho(\varphi, t; \omega_n, \phi_n) = \langle \varphi - \varphi_n \rangle$ in the limit of a large number of oscillators $N \to \infty$ and to consider the associated Fokker–Planck equations

$$\frac{\partial \rho_n}{\partial t} = -\frac{\partial}{\partial \varphi}(\upsilon_n \rho_n) + D\frac{\partial^2 \rho_n}{\partial t^2} \tag{A.1}$$

where $\rho_n(\varphi, t)\,\mathrm{d}\varphi$ gives the probability that the oscillator with frequency ω_n under the action of ϕ_n stays between φ and $\varphi+\mathrm{d}\varphi$ at time t; $\int_0^{2\pi} \rho_n(\varphi, \omega, t)\,\mathrm{d}\varphi = 1$; υ_n is a drift velocity term (cf (4)):

$$\upsilon_n = \dot{\varphi}_n = \omega_n + kr\sin(\psi - \varphi_n) + A_n \sin(\phi_n - \varphi_n). \tag{A.2}$$

The first term on the left in (A.1) is Liouville's continuity condition which states a conservation law for oscillators: if the density is increasing in a certain region there is a corresponding flow into this region from other regions. Continuity condition equations can be combined to obtain a single equation for ρ:

$$\frac{\partial \rho}{\partial t} = -\frac{\partial}{\partial \varphi}\left[\rho\left(\omega + k\int_{-\infty}^{\infty} g(\omega)\,\mathrm{d}\omega \times \int_0^{2\pi} \sin(\varphi' - \varphi)\rho(\varphi', \omega, t)\,\mathrm{d}\varphi'\right)\right]. \tag{A.3}$$

The expression in parentheses above is $\upsilon(\varphi, \omega, t)$ written as the infinite-N version of (3). The last term in (A.1) is the diffusive part spreading out phases of the oscillators.

The stationary solution of (A.1) should satisfy periodic boundary conditions $\rho(\varphi) = \rho(\varphi + 2\pi)$. The trivial solution is $\rho_0 = (2\pi)^{-1}$ with order parameter $r = 0$, which represents incoherence or unsynchronized motion of all oscillators. In the absence of noise ($D = 0$) the condition $\partial\rho_n/\partial t = 0$ implies that $\upsilon_n \rho_n = V_n(\omega, \phi)$ is a constant w.r.t. φ and the solution of (A.1) has a form $\rho_n = V_n/\upsilon_n$, i.e.

$$\rho_n = \frac{V_n}{\omega_n + kr\sin(\psi - \varphi_n) + A_n \sin(\phi_n - \varphi_n)} \tag{A.4}$$

with normalization $V_n = [\int_0^{2\pi} (\upsilon_n(\varphi, \omega, \phi))^{-1}\,\mathrm{d}\varphi]^{-1}$, where υ_n is defined by (A.2). On the other hand, note that the mean field (3) may be written as

$$R = r\mathrm{e}^{\mathrm{i}\psi} = \int_0^{2\pi} \mathrm{e}^{\mathrm{i}\varphi}\left(\frac{1}{N}\sum_{n=1}^{N}\delta(\varphi - \varphi_n)\right)\mathrm{d}\varphi = \frac{1}{N}\sum_{n=1}^{N}\int_0^{2\pi} \mathrm{e}^{\mathrm{i}\varphi}\rho_n(\varphi)\,\mathrm{d}\varphi. \tag{A.5}$$

In the limit $N \to \infty$ and provided all oscillators are initially independent, the mean field in (3) is obtained by averaging over frequency distribution $g(\omega)$ and distribution $f(\phi)$ of the driving phases:

$$r\mathrm{e}^{\mathrm{i}\psi} = \int_{-\infty}^{\infty} g(\omega)\,\mathrm{d}\omega \int_0^{2\pi} f(\phi)\,\mathrm{d}\phi \int_0^{2\pi} \rho(\varphi, \omega, \phi)\mathrm{e}^{\mathrm{i}\varphi}\,\mathrm{d}\varphi. \tag{A.6}$$

If $D = 0$ in (A.1), then ρ is given by (A.4) and (A.6) can be written in the form

$$re^{i\psi} = \frac{1}{P}\int_{-\infty}^{\infty} g(\omega)\,d\omega \int_0^{2\pi} f(\phi)\,d\phi \int_0^{2\pi} \frac{e^{i\varphi}}{\upsilon(\varphi,\omega,\phi)}\,d\varphi \tag{A.7}$$

where normalization constant $P = \int_{-\infty}^{\infty} g(\omega)\,d\omega \int_0^{2\pi} f(\phi)\,d\phi \int_0^{2\pi} (\upsilon(\varphi,\omega,\phi))^{-1}\,d\varphi$.

Equation (A.7) provides the general solution for arbitrary external fields in the absence of noise and may be solved numerically using iterations. Calculations of the order parameter in the presence of noise are more mathematically involved and one may utilize the periodicity of the system and expand the probability density in Fourier series [23] or apply a specific generative functional as in [24].

Appendix B

Let us consider equations of one-dimensional motion of N-coupled NEMS:

$$m\ddot{x}_n + \omega_n^2 x_n - \mu(1 - x_n^2)\dot{x}_n + k_3 x_n^3 + \sum_m h_m(x_n - x_m, \dot{x}_n - \dot{x}_m) = 0. \tag{B.1}$$

The first two terms describe uncoupled harmonic oscillators with frequency ω_n. The third term consists of negative linear dumping $\mu\dot{x}_n$ representing an energy source to sustain the oscillations and positive $\mu x_n^2\dot{x}_n$ dumping, such that oscillations saturate at a limit cycle. The negative dumping can be implemented with an electronic feedback loop sensing oscillator velocity and driving the oscillator phase. The first three terms typically are used to describe MEMS devices. The term $k_3x_n^3$ describes a spring stiffening (Kerr constant $k_3 > 0$) resulting in an amplitude-dependent shift of the resonant frequency which is to be taken into account for NEMS dynamics. The last term presents coupling via displacements $(x_n - x_m)$ typical for elastic or electrostatic interactions; coupling via velocities $(\dot{x}_n - \dot{x}_m)$ introduces dissipation and is not considered here.

With the introduction of a complex variable $z = \dot{x} + i\omega x$ the dynamics of a single oscillator (evolution of its complex state) may be presented as

$$\dot{z} = (c + i\omega)z + (a + ib)z|z|^2 \tag{B.2}$$

where a, b and c are parameters describing stiffness and damping for an oscillating rod clamped on both sides [10].

Based on (B.2) the NEMS dynamics may be presented in polar coordinates $z = re^{i\theta}$ as $\dot{r} = cr + ar^3$; $\dot{\theta} = \omega + br^2$. To get a stable frequency the automatic control level circuitry is to be set such that $b = 0$. To simplify treatment, we may normalize (B.2) with $c = 1$, $a = -1$. For weakly globally coupled oscillators it gives

$$\dot{z}_n = i(\omega_n - b|z_n|^2)z_n + (1 - |z_n|^2)z_n + \frac{k + i\beta}{N}\sum_m (z_m - z_n) \tag{B.3}$$

where b corresponds to nonlinear frequency pulling, k and β are dissipative and reactive parts of all-to-all coupling, respectively. In the case of only nonlinear saturation ($b = 0$) and dissipative coupling ($\beta = 0$, $k \neq 0$) it results in a special case of coupled Landau–Stuart equations [25]:

$$\dot{z}_n = (i\omega_n + 1 - |z_n|^2)z_n + \frac{k}{N}\sum_{m=1}^{N}(z_m - z_n). \tag{B.4}$$

Let us define a complex-valued mean field as

$$\bar{z} = \frac{1}{N}\sum_{m=1}^{N} z_m = r\,e^{\psi}, \tag{B.5}$$

then $\dot{z}_n = (i\omega_n + 1 - |z_n|^2)z_n + k(\bar{z} - z_n)$, or in polar coordinates

$$\dot{r}_n = (1 - r_n^2 - k)r_n + kr\cos(\psi - \theta_n) \tag{B.6}$$

$$\dot{\theta}_n = \omega_n + (kr/r_n)\sin(\psi - \theta_n). \tag{B.7}$$

If coupling is weak (small k) and the width σ_ω of frequency distribution $g(\omega)$ is narrow enough, then r_n rapidly relaxes to a limit cycle with one variable phase θ_n for each array. As the result, the equations are simplified to the Kuramoto model described by (3).

References

[1] Ekinci K and Roukes M 2005 Nano-electromechanical systems *Rev. Sci. Instrum.* **76** 061101

[2] Buks E and Roukes M 2002 Electrically tunable collective response in a coupled micromechanical array *J. Microelectromech. Syst.* **11** 802–7

[3] Sapmaz S, Blanter Y, Gurevich L and van der Zant H 2003 Carbon nanotubes as nanoelectromechanical systems *Phys. Rev.* B **67** 236414

[4] Yu M-F, Wagner G, Ruoff R and Dyer M 2002 Realization of parametric resonances in a nanowire mechanical system with nanomanipulation inside a scanning electron microscope *Phys. Rev.* B **66** 073406

[5] Kinaret J, Nord T and Viefers S 2003 A carbon-nanotube-based nanorelay *Appl. Phys. Lett.* **82** 1287–9

[6] Zheng Q and Jiang Q 2002 Multiwalled carbon nanotubes as Gigahertz oscillators *Phys. Rev. Lett.* **88** 045503

[7] Legoas S, Coluci V, Braga S, Coura P, Dantas S and Galvao D 2003 Molecular-dynamics simulations of carbon nanotubes as Gigahertz oscillators *Phys. Rev. Lett.* **90** 045504

[8] Aubin K, Zalalutdinov M, Alan T, Reichenbach R, Rand R, Zehnder A, Parpia J and Craighead H 2004 Limit cycle oscillations in CW laser-driven NEMS *IEEE J. Micromech. Syst.* **13** 1018–26

[9] Sazonova V, Yaish Y, Uesteenel H, Roundy D, Arias T and McEuen P 2004 A tunable carbon nanotube electromechanical oscillator *Nature* **431** 286–7

[10] Hoppensteadt F and Izhikevich E 2001 Synchronization of MEMS resonators and mechanical neurocomputing *IEEE Trans. Circuits Syst.* I **48** 133–8

[11] Strogatz S 2003 *Sync: The Emerging Science of Spontaneous Order* (New York: Hyperion)

[12] Haykin S 2005 Cognitive radio: brain-empowered wireless communications *IEEE J. Sel. Areas Commun.* **23** (Feb) 201–20

[13] Nefedov N 2007 Spectral sensing with coupled nanoscale resonators *Int. Conf. Nano Networks (Catania)*

[14] Kuramoto Y 1975 *Lecture Notes in Phys.* vol 30 (Berlin: Springer)

[15] Acebron J, Bonilla L, Vicente C and Ritort F 2005 The Kuramoto model: a simple paradigm for synchronization phenomena *Rev. Mod. Phys.* **77** 137–85
[16] Hoppensteadt F C and Izhikevich E M 1997 *Weakly Connected Neural Networks* vol 126 (Berlin: Springer)
[17] Tsimring L, Rulkov N, Larsen M and Gabbay M 2005 Repulsive synchronization in an array of phase oscillators *Phys. Rev. Lett.* **95** 014101
[18] Rulkov N, Tsimring L, Larsen M and Gabbay M 2006 Synchronization and beam forming in an array of repulsively coupled oscillators *Phys. Rev.* E **74** 056205
[19] Watanabe S and Strogatz S 1994 Constants of motion for superconducting Josephson arrays *Physica* D **74** 197–253
[20] Wiesenfeld K and Swift J 1995 Averaged equations for Josephson junction series arrays *Phys. Rev.* E **51** 1020–4
[21] Shim S-B, Imboden M and Mohanty P 2007 Synchronized oscillation in coupled nanomechanical oscillators *Science* **316** 95–9
[22] Peng H, Chang C, Aloni S, Yuzvinsky T and Zettl A 2007 Microwave electromechanical resonator consisting of clamped carbon nanotubes in an abacus arrangement *Phys. Rev.* B **76** 03540
[23] Hong H, Choi M, Park K, Yoon B-G and Soh K-S 1999 Synchronization and resonance in a driven system of coupled oscillators *Phys. Rev.* E **60** 4014–20
[24] Arenas A and Vicente P 1994 Exact long-time behavior of a network of phase oscillators under random fields *Phys. Rev.* E **50** 949–56
[25] Aranson I and Kramer L 2002 The world of the complex Ginzburg–Landau equation *Rev. Mod. Phys.* **74** 99–143